Title: Distorted Local Shadows

Date: Sep 24, 2015 01:00 PM

URL: http://pirsa.org/15090022

Abstract: <p>We introduce the notion of a local shadow for a black hole and determine its shape for the particular case of a distorted Schwarzschild black hole. Considering the lowest-order even and odd multiple moments, we compute the relation between the deformations of the shadow of a Schwarzschild black hole and the distortion multiple moments. For the range of values of multiple moments that we consider, the horizon is deformed much less than its corresponding shadow, suggesting the horizon is more `rigid'. Quite unexpectedly we find that a prolate distortion of the horizon gives rise to an oblate distortion of the shadow, and vice-versa.</p>

Distorted Local Shadows

Christos Tzounis

Theoretical Physics Institute,
University of Alberta

September 24, 2015

Distorted local shadows, Shohreh Abdolrahimi, Robert B. Mann, and Christos Tzounis, Phys. Rev. D **91**, 084052 (2015).

Overview

Background

Black Hole Shadow

Background: Black Hole Shadow

What is the Shadow of a Black Hole?

Although a black hole is not visible, we can observe it nonetheless when it casts a shadow if it is in front of a bright background.

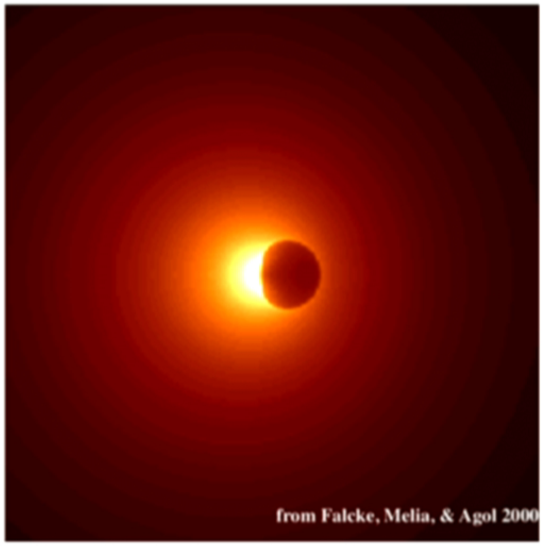

Background: Black Hole Shadow

The original investigation of the shadow of a Schwarzschild black hole [J. L. Synge, (1966)] has been extended to a number of other cases [J. Bardeen, (1973), A. de Vries, (2000), C. T. Cunningham, et al., (1973), J.W. Moffat (2015)].

Shadow of a Schwarzschild black hole

A circle of radius $3\sqrt{3}M$ which corresponds to the specific angular momentum, $(l \equiv \tilde{L}/\mathcal{E})$, of the knife-edge orbit.

Why is the Shadow of a Black Hole important?

- Information about their spin, mass and their charge.
- Test for general relativity. For example, propagation of light in a curved background.

References

J. L. Synge, (1966).
The escape of photons from gravitationally intense stars.
Mon. Not. R. Astron. Soc. **131** *463.*

J. Bardeen, (1973).
Timelike and null geodesics in the Kerr metric
Black Holes. cole d't de Physique Thorique, Les Houches 1972, 215-239.

C. T. Cunningham and J. M. Bardeen, (1973)
The optical appearance of a star orbiting an extreme Kerr black hole.
ApJ **183** *237*

A. de Vries, (2000).
The apparent shape of a rotating charged black hole, closed photon orbits and the bifurcation set A_4.
Class. Quantum Grav. **17** *123*

J.W. Moffat, (2015).
Black holes in modified gravity (MOG).
European Physical Journal C 75:175 .

Background: Distorted Black Holes

What is a Distorted Black Hole?

A distorted black hole describes a non-isolated black hole by an exact, local solution, which is physically relevant only in a close neighbourhood of the horizon.
The solution can be interpreted as describing locally a black hole distorted by external matter.

Why is a Distorted Black Hole important?

- It is an exact solution.
- It is a "photograph" of dynamical systems.
- Information about the surrounding matter.
- We can test how universal are the black holes properties. An example is the spin of a Kerr black hole.

Main Questions

- What is the apparent shape, (shadow), of a distorted black hole?
- How the external matter that manifests itself into the black modifies the propagation of light?
- Is there a connection between the shape of the shadow and the shape of the horizon?

Set Up

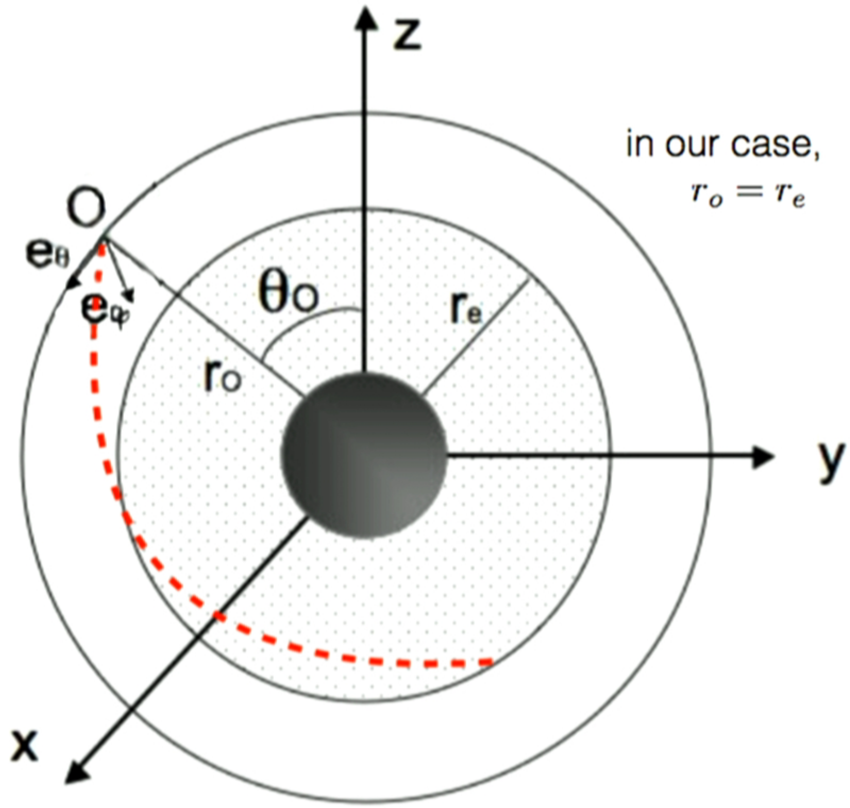

in our case,

$r_o = r_e$

Spacetime metric and map

Metric

Spacetime metric and map

Metric

$$dS^2 = -\left(1-\frac{2M}{\rho}\right)e^{2U}d\mathcal{T}^2 + \left(1-\frac{2M}{\rho}\right)^{-1}e^{-2U+2V}d\rho^2 + e^{-2U}\rho^2(e^{2V}d\theta^2 + \sin^2\theta d\phi^2)\,. \quad (1)$$

where, $U = U(\rho,\theta)$ and $V = V(\rho,\theta)$ are functions of ρ and θ.

Spacetime metric and map

$$d\mathcal{S}^2 = r_g^2 dS^2, \quad T = \frac{\mathcal{T}}{r_g}, \quad \rho = r_g r, \tag{2}$$

$$\mathcal{U} = U - u_0, \quad u_0 = \sum_{n\geq 0} c_{2n}, \quad t = Te^{2u_0} \tag{3}$$

Spacetime metric and map

$$d\mathcal{S}^2 = r_g^2 dS^2, \quad T = \frac{\mathcal{T}}{r_g}, \quad \rho = r_g r, \tag{2}$$

$$\mathcal{U} = U - u_0, \quad u_0 = \sum_{n\geq 0} c_{2n}, \quad t = Te^{2u_0} \tag{3}$$

Conformal metric

$$\begin{aligned} ds^2 &= -(1-\frac{1}{r})e^{2\mathcal{U}}dt^2 + (1-\frac{1}{r})^{-1} e^{-2\mathcal{U}+2V}dr^2 \\ &+e^{-2\mathcal{U}}r^2(e^{2V}d\theta^2 + \sin^2\theta d\phi^2), \end{aligned} \tag{4}$$

Spacetime metric and map

Conformal metric

$$ds^2 = -(1-\frac{1}{r})e^{2\mathcal{U}}dt^2 + (1-\frac{1}{r})^{-1} e^{-2\mathcal{U}+2V}dr^2 + e^{-2\mathcal{U}}r^2(e^{2V}d\theta^2 + \sin^2\theta d\phi^2)$$

This spacetime has the following two constants of motion,

$$E \equiv -u_\mu \xi^\mu_{(t)} = \left(1-\frac{1}{r}\right) e^{2\mathcal{U}}\,\dot{t}\,,$$
$$L_z \equiv u_\mu \xi^\mu_{(\phi)} = e^{-2\mathcal{U}} r^2 \sin^2\theta\,\dot{\phi} \qquad (5)$$

Spacetime metric and map

Distorting potentials

$$
\begin{aligned}
U &= \sum_{n\geq 0} c_n R^n P_n \\
V &= \sum_{n\geq 1} c_n \sum_{l\geq 0}^{n-1} \left[\cos\theta - (2r-1) - (-1)^{n-l}((2r-1)+\cos\theta)\right] R^l P_l \\
&+ \sum_{n,k\geq 1} \frac{nkc_n c_k}{n+k} R^{n+k}(P_n P_k - P_{n-1}P_{k-1}) \qquad (6)
\end{aligned}
$$

where,

$$
\begin{aligned}
P_n &= P_n((2r-1)\frac{\cos\theta}{R}) \\
R &= \sqrt{(2r-1)^2 - \sin^2\theta}. \qquad (7)
\end{aligned}
$$

Spacetime metric and map

When radius ρ of the observation point is less than the radius of the mass source.

Expansion of the Newtonian potential in terms of Legendre polynomials:

$$\Phi = G \sum_{n=0}^{\infty} \tilde{c}_n P_n(\cos\theta) \rho^n \,. \tag{8}$$

$\tilde{c}_n$'s are the interior Newtonian multiple moments and θ is the observation angle.

We can relate $\tilde{c}_n$ with c_n

Example:

$$c_0 = \tilde{c}_0 - \frac{M^2}{24}\tilde{c}_2 \,, \qquad c_1 = -c_3 = -\frac{M^3}{32}\tilde{c}_3 \,, \tag{9}$$

$$c_2 = \frac{M^2}{8}\tilde{c}_2 \,. \tag{10}$$

Spacetime metric and map

Map

Spacetime metric and map

First we choose the following orthonormal tetrad

$$e_0^\mu = \frac{1}{\sqrt{(1-\frac{1}{r})f}}\delta_t^\mu\Big|_o, \quad e_1^\mu = \sqrt{\frac{1}{h}(1-\frac{1}{r})}\delta_r^\mu\Big|_o,$$

$$e_2^\mu = \frac{1}{r\sqrt{h}}\delta_\theta^\mu\Big|_o, \quad e_3^\mu = \frac{\sqrt{f}}{r\sin\theta}\delta_\phi^\mu\Big|_o. \tag{11}$$

at the point of the observation, where $...\Big|_o$ stands for the limit where $r = r_o$ and $\theta = \theta_o$.

The tangent vector to a null ray is

$$u^\mu = \frac{dx^\mu}{d\tau}. \tag{12}$$

If we project this vector into the observer's orthonormal frame. We get,

$$u^\mu = \beta(-e_0^\mu + \xi^1 e_1^\mu + \xi^2 e_2^\mu + \xi^3 e_3^\mu), \tag{13}$$

where ξ^2, and ξ^3 are displacement angles.

Spacetime metric and map

Replacing Eq.(11) (orthonormal tetrad) in Eq.(13) and comparing to Eq.(12) and using Eq.(5) (constants of motion), we find the value of the scalar coefficient β

$$\beta = -\frac{E}{\sqrt{(1-\frac{1}{r})f}}. \tag{14}$$

Replacing Eq.(11) in Eq.(13) and comparing to Eq.(12), we find the displacement angles ξ^2, and ξ^3 and using Eq.(14). Moreover, by multiplying by r_o and we find,

$$\bar{\xi}^2 = \pm\frac{l_z}{\sin^2\theta} f^{\frac{3}{2}} \sqrt{h(1-\frac{1}{r})}\theta'\Big|_o,$$
$$\bar{\xi}^3 = -\frac{l_z}{\sin\theta} f \sqrt{1-\frac{1}{r}}\Big|_o. \tag{15}$$

Spacetime metric and map

$$\bar{\xi}^2 = \pm \frac{l_z}{\sin^2\theta} f^{\frac{3}{2}} \sqrt{h(1-\frac{1}{r})\theta'}\Big|_o ,$$
$$\bar{\xi}^3 = -\frac{l_z}{\sin\theta} f \sqrt{1-\frac{1}{r}}\Big|_o . \quad (16)$$

where,

$$l_z \equiv \frac{L_z}{E} .$$

For this map we used the following two equations,

$$\dot{r} = \frac{dr}{d\tau} = \frac{dr}{d\phi}\frac{d\phi}{d\tau} = r'\dot{\phi} ,$$
$$\dot{\theta} = \frac{d\theta}{d\tau} = \frac{d\theta}{d\phi}\frac{d\phi}{d\tau} = \theta'\dot{\phi} . \quad (17)$$

Technical details: Choice of multiple moments

What is the right value of multiple moments?

For simplicity we consider the lowest order multiple moments (considering odd and even moments separately). In choosing the appropriate value of multiple moment, we suppose its value to be small enough that the ratio $f = g_{tt\mathrm{d}}/g_{tt}$ of the tt-component of the distorted black hole metric to its Schwarzschild counterpart is not very large, i.e., $f < 10$.

Example:
For $c_1 = 1/150$ is a very strong distortion, such that $g_{tt\mathrm{d}}/g_{tt} > 10000$.

Technical details: Choice of multiple moments

Value of multiple moments

We need to keep in mind that we want to consider a black hole distorted by external sources that are not much stronger gravitationally than the black hole itself.

$-1/150 < c_2 < 1/150$; for this range of values of c_2 we have, $g_{ttd}/g_{tt} < 2.6$.

$-1/800 < c_1 < 1/800$; we find $g_{ttd}/g_{tt} < 6$ for this range of values of $c_1 = -c_3$.

Page 40 of 105

Technical details: Choice of multiple moments

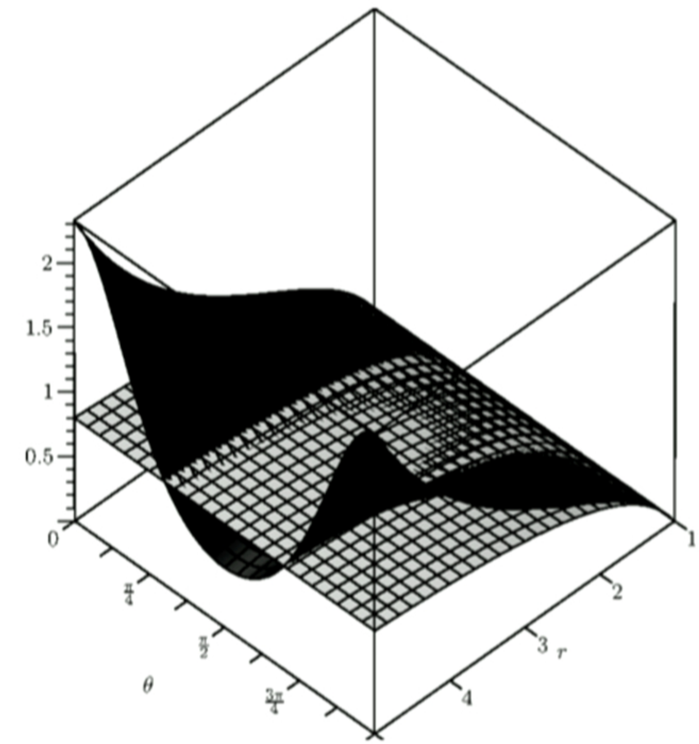

Figure : Comparison of g_{ttd} of the distorted black hole (black), to g_{tt} of the Schwarzschild black hole (grey). For $c_2 = 1/150$.

Technical details: Choice of multiple moments

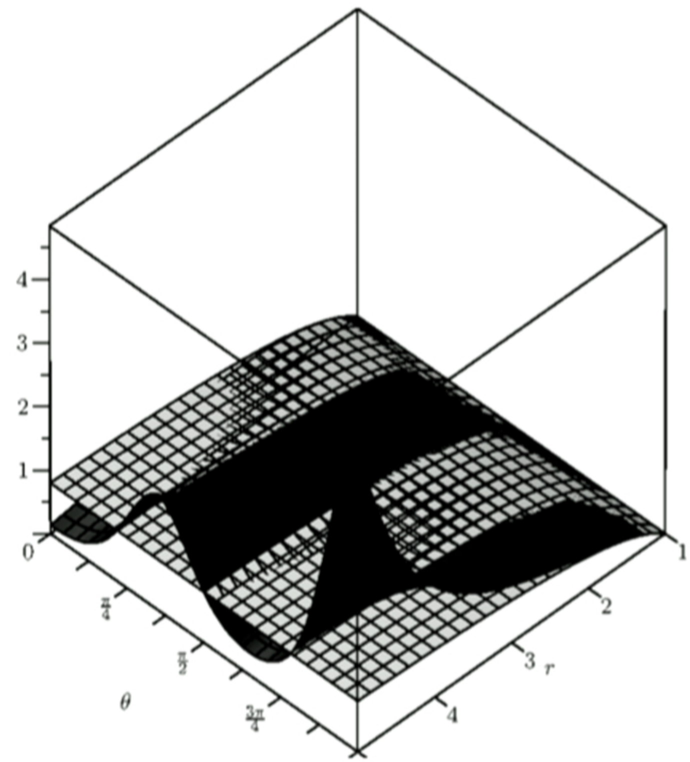

Figure : Comparison of g_{ttd} of the distorted black hole (black), to g_{tt} of the Schwarzschild black hole (grey). For $c_1 = 1/800$.

Technical details

Numerical computation

Technical details: Numerical computation

$$u_\mu u^\nu = 0 \Rightarrow \tag{18}$$

$$\Rightarrow r' = \left[\frac{r^4 \sin^4\theta}{f^3 l_z^2 h} - \frac{r^2 \sin^2\theta}{fh}(1-\frac{1}{r}) - r^2\theta'^2(1-\frac{1}{r})\right]^{\frac{1}{2}} \tag{19}$$

$$\Rightarrow r'(r_o, \theta_o) = \sqrt{\frac{r^2 \sin^4\theta}{f^3 l_z^2 h}}\Big|_{(r_o,\theta_o)} \sqrt{r_o^2 - (\bar{\xi}^3)^2 - (\bar{\xi}^2)^2} \tag{20}$$

From the constraint above gives us the range of values of $\bar{\xi}^3$ and $\bar{\xi}^2$ that are valid.

Numerically, we divide the interior region of the circle of Eq.(20) to small pixels of side 0.01.

For each trajectory, we calculate the maximum deviation from the constraint Eq.(18). From this we find the maximum deviation from the constraint for all the trajectories, which we find to be 4×10^{-4}.

Results and Discussion

Odd multiple moments

Results and Discussion: Odd multiple moments

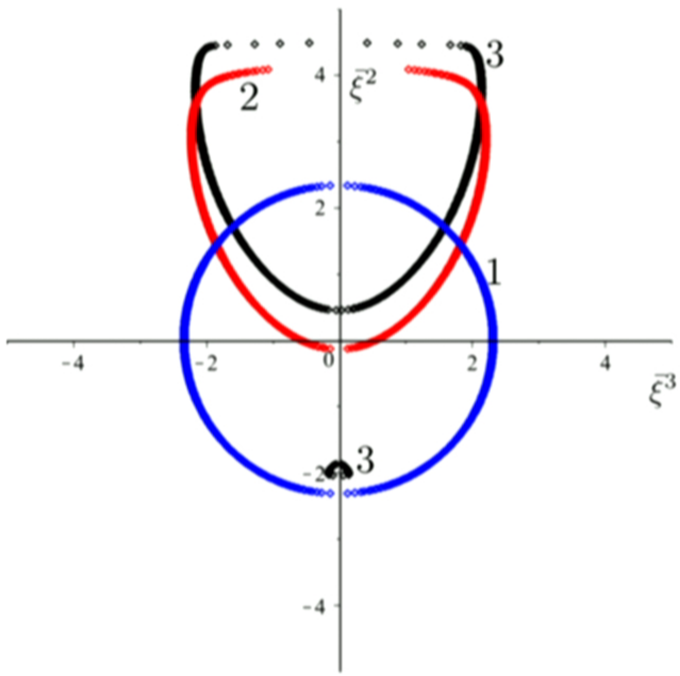

Figure : The shadow of a black hole for an observer at $\theta_o = \pi/2$ and radius $r_o = 5$; the values of the multiple moments are $c_1 = \frac{1}{1000}$, (with red, (2)) $c_1 = \frac{1}{800}$, (with black, (3)) and $c_1 = 0$, (which is the undistorted case with blue, (1)).

Results and Discussion: Odd multiple moments

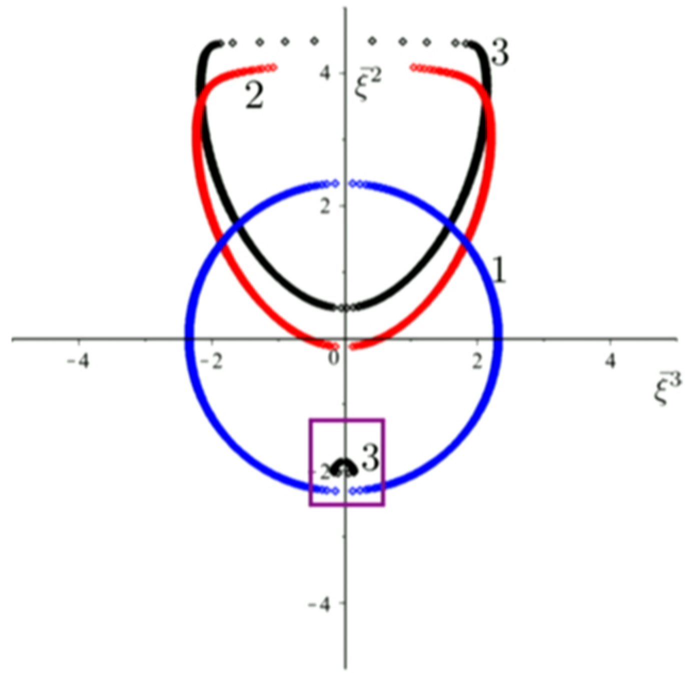

Results and Discussion: Odd multiple moments

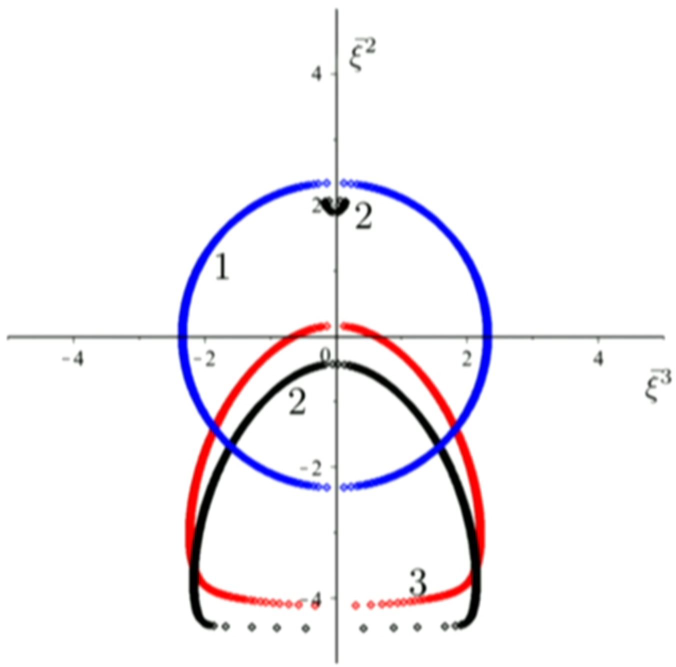

Figure : The shadow of a black hole for an observer at $\theta_o = \pi/2$ and radius $r_o = 5$; the values of the multiple moments are $c_1 = -\frac{1}{1000}$, (with red, (3)) $c_1 = -\frac{1}{800}$, (with black, (2)) and $c_1 = 0$, (which is the undistorted case with blue, (1)).

Results and Discussion: Odd multiple moments

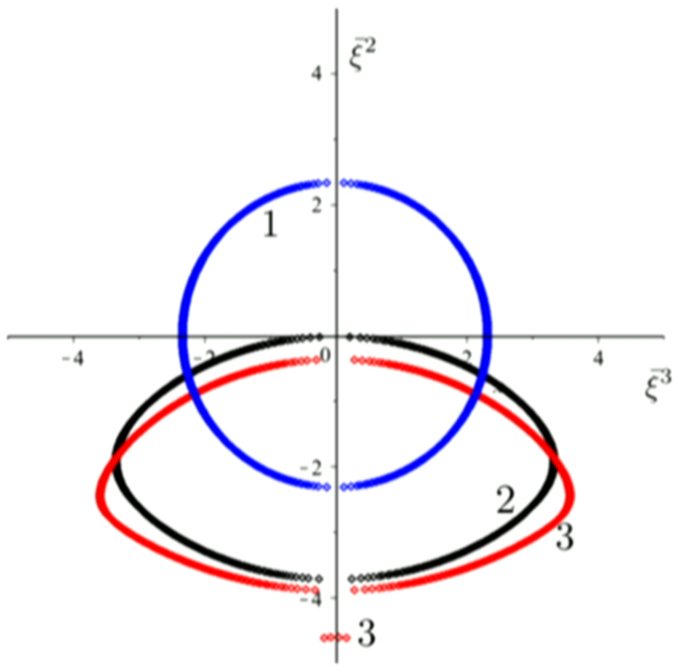

Figure : The shadow of a black hole for an observer at $\theta_o = \pi/4$ and radius $r_o = 5$; the values of the multiple moments are $c_1 = \frac{1}{800}$, (with red, (3)) $c_1 = \frac{1}{1000}$, (with black, (2)) and $c_1 = 0$, (which is the undistorted case with blue, (1)).

Results and Discussion: Odd multiple moments

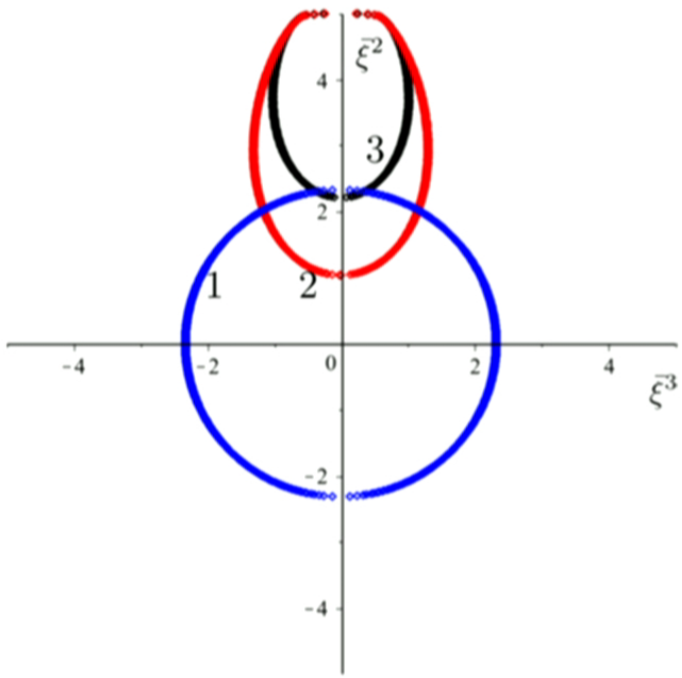

Figure : The shadow of a black hole for an observer at $\theta_o = \pi/4$ and radius $r_o = 5$; the values of the multiple moments are $c_1 = -\frac{1}{1000}$, (with red, (2)) $c_1 = -\frac{1}{800}$, (with black, (3)) and $c_1 = 0$, (which is the undistorted case with blue, (1)).

Results and Discussion: Odd multiple moments

For odd multiple moment c_1, we observe an "eyebrow" structure for large values of multiple moments (e.g. $c_1 = 1/800$), reminiscent of those seen for the shadow of two merging black holes [R. Cowen, (2014)].
For an observer in the equatorial plane the shadow looks like an incomplete ellipse that is flattened on one side.
Mirror-reflected with respect to the $\bar{\xi}^3$ axis upon changing the sign of the multipole moment from positive to negative.

R. Cowen, (2014).
Black-hole mergers cast kaleidoscope of shadows.
Nature 16283.

Results and Discussion: Odd multiple moments

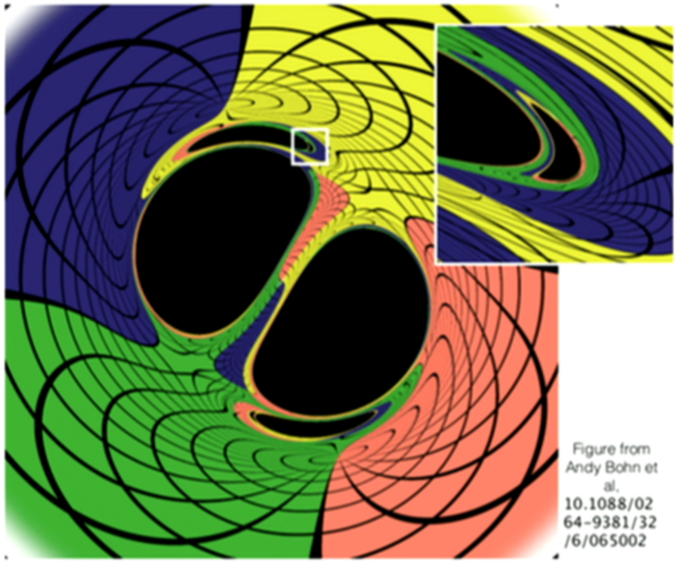

Figure from Andy Bohn et al. 10.1088/0264-9381/32/6/065002

Results and Discussion: Odd multiple moments

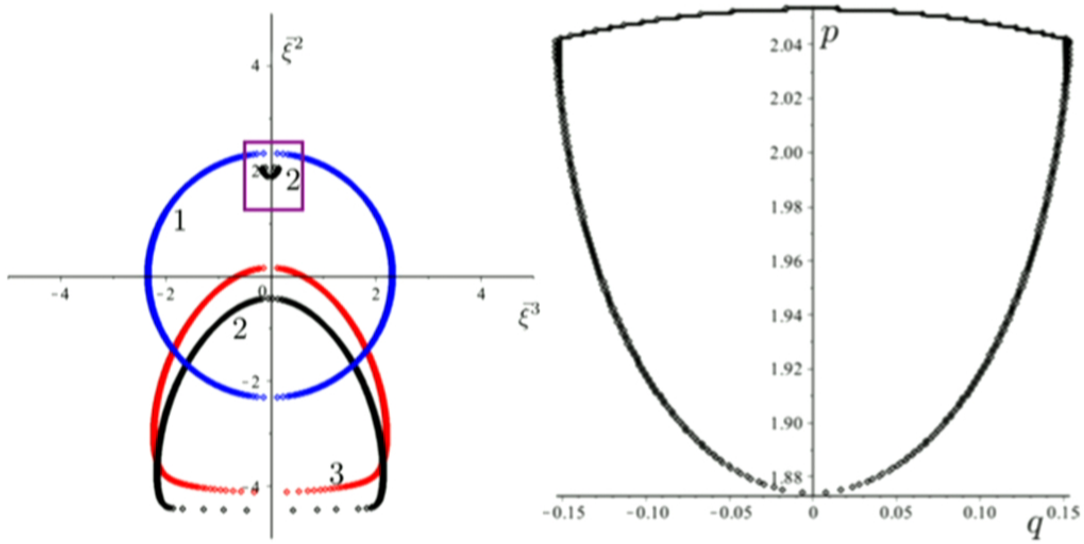

Figure : Zoom to the eyebrow structure for case of $c_1 = -1/800$. The observer is located on the equator and $r_o = 5$.

Results and Discussion: Odd multiple moments

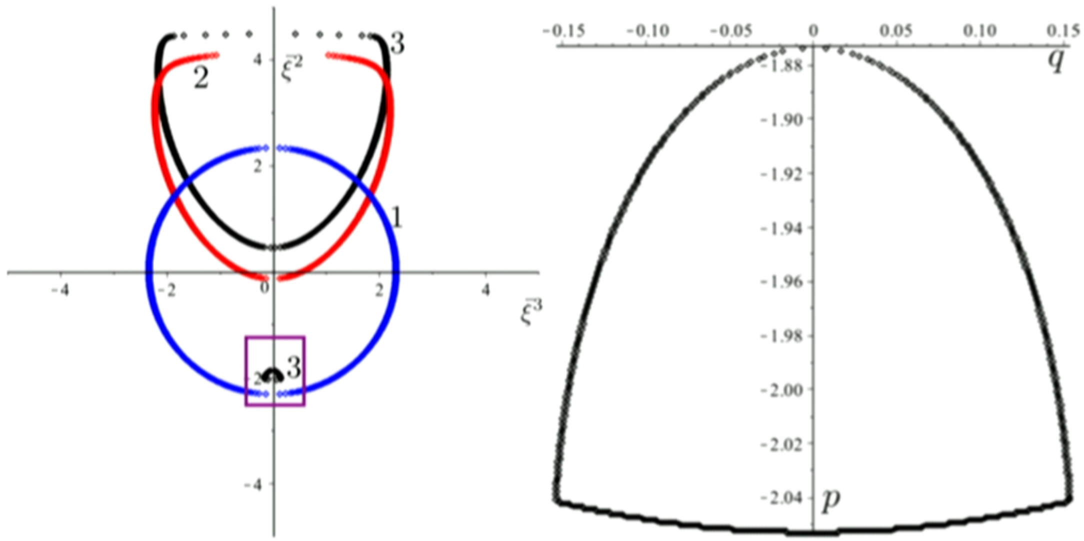

Figure : Zoom to the eyebrow structure for case of $c_1 = 1/800$. The observer is located on the equator and $r_o = 5$.

Results and Discussion: Odd multiple moments

For odd multiple moment c_1, the "eyebrow" has the same shape as the "primary shadow ". However, is smaller and a mirror reflection of the "primary image " with respect to $\bar{\xi}^3$ axis.

Results and Discussion: Even multiple moments

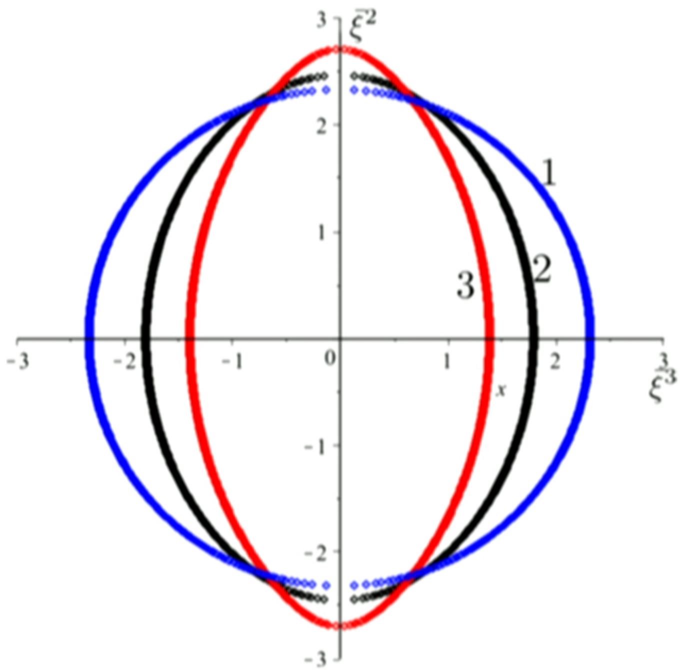

Figure : The shadow of a black hole for an observer at $\theta_o = \pi/2$ and radius $r_o = 5$; the values of the multiple moments are $c_2 = \frac{1}{150}$, (with red, (3)) $c_2 = \frac{1}{300}$, (with black, (2)) and $c_2 = 0$, (which is the undistorted case with blue, (1)).

Page 61 of 105

Results and Discussion: Even multiple moments

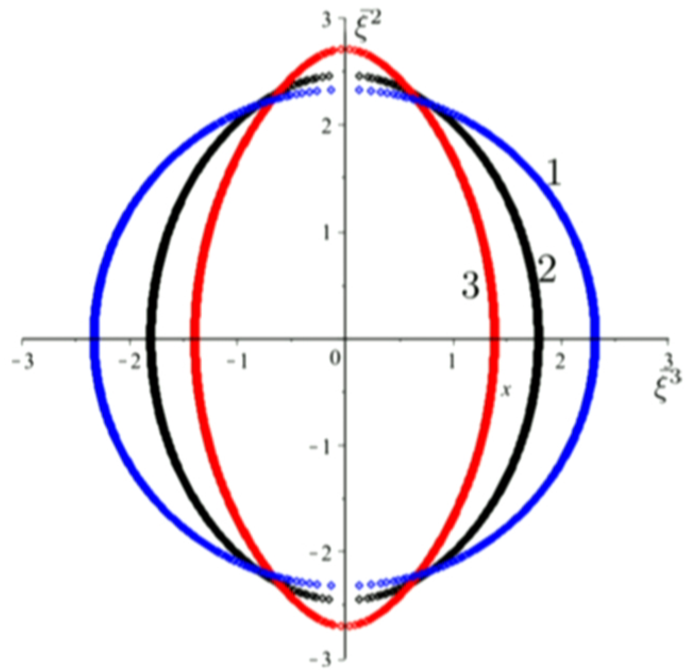

Figure : The shadow of a black hole for an observer at $\theta_o = \pi/2$ and radius $r_o = 5$; the values of the multiple moments are $c_2 = \frac{1}{150}$, (with red, (3)) $c_2 = \frac{1}{300}$, (with black, (2)) and $c_2 = 0$, (which is the undistorted case with blue, (1)).

Results and Discussion: Even multiple moments

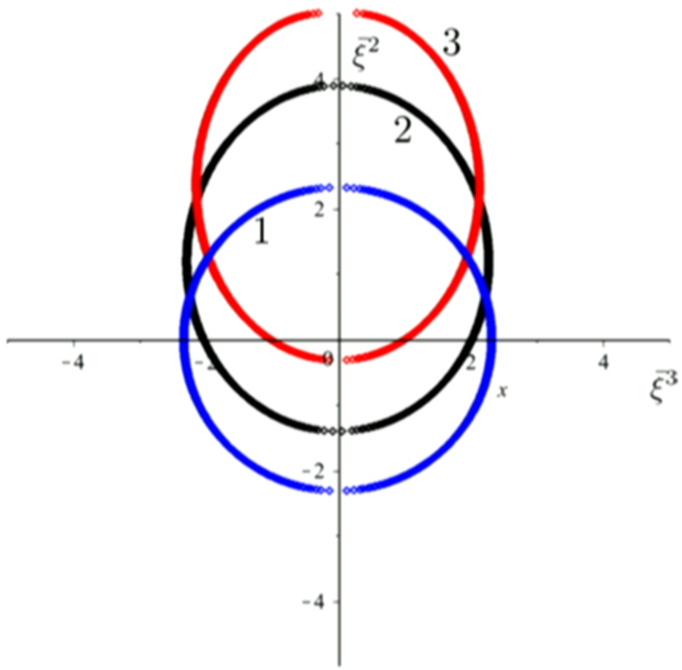

Figure : The shadow of a black hole for an observer at $\theta_o = \pi/4$ and radius $r_o = 5$; the values of the multiple moments are $c_2 = \frac{1}{150}$, (with red, (3)) $c_2 = \frac{1}{300}$, (with black, (2)) and $c_2 = 0$, (which is the undistorted case with blue, (1)).

Results and Discussion: Even multiple moments

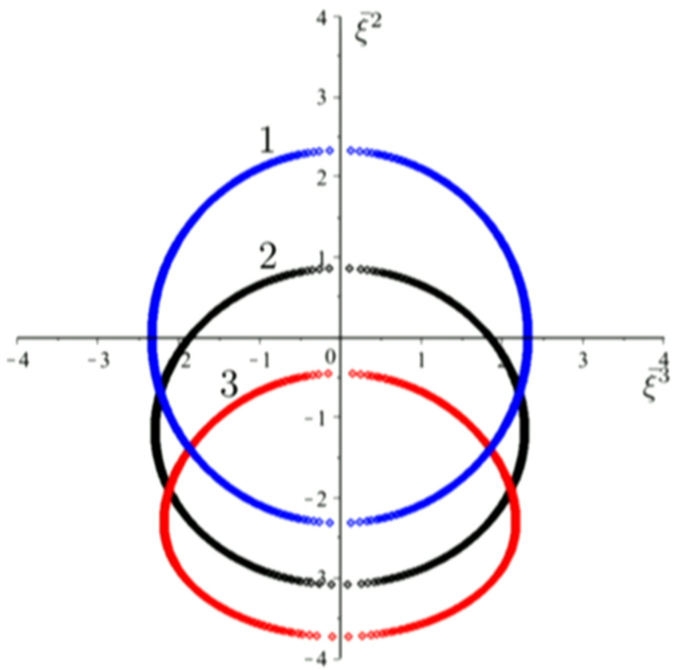

Figure : The shadow of a black hole for an observer at $\theta_o = \pi/4$ and radius $r_o = 5$; the values of the multiple moments are $c_2 = -\frac{1}{150}$, (with red, (3)) $c_2 = -\frac{1}{300}$, (with black, (2)) and $c_2 = 0$, (which is the undistorted case with blue, (1)).

Results and Discussion: Even multiple moments

For $\theta_o = \pi/2$, we fit the shape of the shadow to an ellipse, taking a and b to be its semi-major/semi-minor axes, the origin at the centre, and the angular coordinate ϕ to be measured from the axis $\bar{\xi}^3$.

Results and Discussion: Even multiple moments

For $\theta_o = \pi/2$, we fit the shape of the shadow to an ellipse, taking a and b to be its semi-major/semi-minor axes, the origin at the centre, and the angular coordinate ϕ to be measured from the axis $\bar{\xi}^3$.

To find a and b we minimize the normalized square error

$$J = \frac{\sum_{i=0}^{m}(\rho_i^{\text{numer}} - \rho_i)^2}{\sum_{i=0}^{m}(\rho_i^{\text{numer}})^2}, \tag{21}$$

with

$$\rho_i^{\text{numer}} = [(\bar{\xi}^3)^2 + (\bar{\xi}^2)^2]^{1/2},$$
$$\rho_i = \frac{ab}{\sqrt{b^2\cos^2\phi_i + a^2\sin^2\phi_i}},$$
$$\phi_i = \arctan\left(\frac{\bar{\xi}^2}{\bar{\xi}^3}\right), \tag{22}$$

where ρ_i^{numer} is given by our numerical result, and ρ_i is the equation of the ellipse for every ϕ_i.

Results and Discussion: Even multiple moments

For $\theta_o = \pi/2$, we fit the shape of the shadow to an ellipse, taking a and b to be its semi-major/semi-minor axes, the origin at the centre, and the angular coordinate ϕ to be measured from the axis $\bar{\xi}^3$.

To find a and b we minimize the normalized square error

$$J = \frac{\sum_{i=0}^{m}(\rho_i^{\text{numer}} - \rho_i)^2}{\sum_{i=0}^{m}(\rho_i^{\text{numer}})^2}, \quad (21)$$

with

$$\rho_i^{\text{numer}} = [(\bar{\xi}^3)^2 + (\bar{\xi}^2)^2]^{1/2},$$
$$\rho_i = \frac{ab}{\sqrt{b^2\cos^2\phi_i + a^2\sin^2\phi_i}},$$
$$\phi_i = \arctan\left(\frac{\bar{\xi}^2}{\bar{\xi}^3}\right), \quad (22)$$

where ρ_i^{numer} is given by our numerical result, and ρ_i is the equation of the ellipse for every ϕ_i.

Results and Discussion: Even multiple moments

r_o	b	**error in b fitting**
3	$b = 8.89c_2 + 2.12$	7.25×10^{-4}
4	$b = 22.58c_2 + 2.25$	1.1×10^{-6}
5	$b = 34.11c_2 + 2.32$	1.2×10^{-4}
6	$b = 44.27c_2 + 2.37$	3.3×10^{-5}

Table : Obtained values and errors of the parameter b for an observer on the equatorial plane at r_o.

r_o	a	**error in a fitting**
3	$a = -41.85c_2 + 2.12$	1.34×10^{-4}
4	$a = -99.68c_2 + 2.25$	4.3×10^{-4}
5	$a = -161.96c_2 + 2.32$	3.5×10^{-2}
6	$a = -251.63c_2 + 2.37$	2.4×10^{-2}

Table : Obtained values and errors of the parameter a for an observer on the equatorial plane at r_o.

Results and Discussion: Even multiple moments

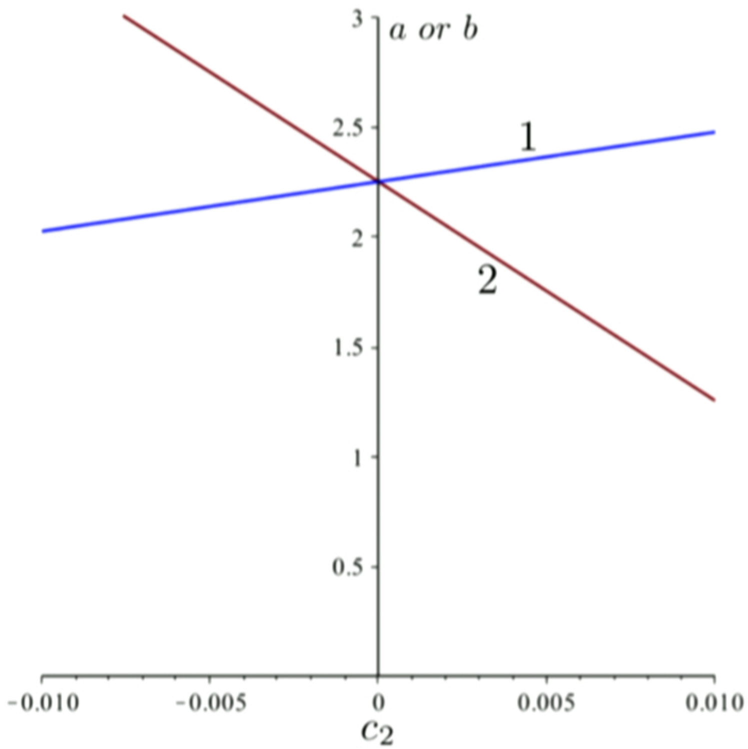

Figure : The parameters of the ellipse a (red, (2)) and b (blue, (1)) vs. the multiple moment c_2, for observer at $r_o = 4$.

Results and Discussion: Even multiple moments

The horizon surface, $t = \text{const}$, $r = 1$, of the distorted black hole Eq.(4) is given by

$$dS_H^2 = e^{-2\mathcal{U}_H}(e^{2V_H}d\theta^2 + \sin^2\theta d\phi^2) \tag{23}$$

where, $\mathcal{U}_H = \mathcal{U}(r = 1, \theta)$ and $V_H = V(r = 1, \theta)$. Consider isometrically embedding this 2-dimensional axisymmetric metric into the 3-dimensional space

$$ds^2 = \epsilon dZ^2 + d\rho^2 + \rho^2 d\phi^2 \tag{24}$$

where (Z, ρ, ϕ) are cylindrical coordinates. Setting $\epsilon = 1$ corresponds to Euclidean space, whereas $\epsilon = -1$ corresponds to pseudo-Euclidean space. We have $Z = Z(\theta)$, and $\rho = \rho(\theta)$.

Results and Discussion: Even multiple moments

Matching the metrics (23) and (24), we derive the following embedding map

$$\rho(\theta) = e^{-\mathcal{U}_H} \sin\theta,$$
$$Z(\theta) = \int_{\theta}^{\pi/2} \left[\epsilon\left(e^{-2\mathcal{U}_H + 2V_H} - \rho_{,\theta'}^2\right)\right]^{\frac{1}{2}} d\theta'. \quad (25)$$

For even multiple moments the horizon is deformed to an ellipse. Using the same fitting method as before, we find

$$a = 1.07c_2 + 1, \quad b = -2.11c_2 + 1 \quad (26)$$

where we have fixed the intercept of the linear fit to be 1 and found the slope; the errors in the above fittings are of order 10^{-5}.

Results and Discussion: Even multiple moments

r_o	b	**error in b fitting**
3	$b = 8.89c_2 + 2.12$	7.25×10^{-4}
4	$b = 22.58c_2 + 2.25$	1.1×10^{-6}
5	$b = 34.11c_2 + 2.32$	1.2×10^{-4}
6	$b = 44.27c_2 + 2.37$	3.3×10^{-5}

Table : Obtained values and errors of the parameter b for an observer on the equatorial plane at r_o.

r_o	a	**error in a fitting**
3	$a = -41.85c_2 + 2.12$	1.34×10^{-4}
4	$a = -99.68c_2 + 2.25$	4.3×10^{-4}
5	$a = -161.96c_2 + 2.32$	3.5×10^{-2}
6	$a = -251.63c_2 + 2.37$	2.4×10^{-2}

Table : Obtained values and errors of the parameter a for an observer on the equatorial plane at r_o.

Results and Discussion: Even multiple moments

→ $c_2 > 0$ the horizon of the black hole is oblate but, its shadow is prolate.
→ $c_2 < 0$ the opposite occurs: a prolate horizon has an oblate shadow.
For a quadrupole moment c_2 the equations of motion imply that on the equatorial plane $\ddot{\theta} = 0$ when $\dot{\theta} = 0$.
The equations of motion are integrable on the equator therefore, we can construct an effective potential V for the planar motion of null rays.

$$\frac{1}{l_z^2}\left(\frac{d\tilde{r}}{d\tilde{t}}\right)^2 = \frac{1}{l_z^2} - V^2, \tag{27}$$

where

$$V^2 = \frac{1}{r^2}\left(1 - \frac{1}{r}\right)f^2,$$

$$d\tilde{t} = \left[f\left(1 - \frac{1}{r}\right)\right]^{1/2}, \qquad d\tilde{r} = \left[h\left(1 - \frac{1}{r}\right)^{-1}\right]^{1/2}. \tag{28}$$

The maximum of the effective potential is equal to the value of $1/l_z^2$ or $1/b^2_{critical}$ for the knife-edge orbit.

Results and Discussion: Even multiple moments

For $c_2 = 1/150$ we have $1/b^2_{critical} = 0.1389$.
Using our map,

$$\bar{\xi}^2 = \pm \frac{l_z}{\sin^2\theta} f^{\frac{3}{2}} \sqrt{h(1-\frac{1}{r})\theta'}\Big|_o,$$
$$\bar{\xi}^3 = -\frac{l_z}{\sin\theta} f \sqrt{1-\frac{1}{r}}\Big|_o. \quad (29)$$

for an observer located on the equator and $r_o = 5$ we get,

$$\bar{\xi}^3 = 1.3894\,.$$

Undistorted Schwarzschild black hole, for which $\bar{\xi}^3 = 2.32$.

Results and Discussion: Even multiple moments

For $c_2 > 0$:
→ Equator: $g_{ttd} < g_{tt}$,
→ Axis: $g_{ttd} > g_{tt}$.

Results and Discussion: Even multiple moments

The angular momentum of the photons for the knife edge orbit is larger than the undistorted case. Therefore, if instead of the map,

$$\bar{\xi}^2 = \pm \frac{l_z}{\sin^2\theta} f^{\frac{3}{2}} \sqrt{h(1-\frac{1}{r})\theta'}\Big|_o,$$
$$\bar{\xi}^3 = -\frac{l_z}{\sin\theta} f \sqrt{1-\frac{1}{r}}\Big|_o. \tag{30}$$

Results and Discussion: Even multiple moments

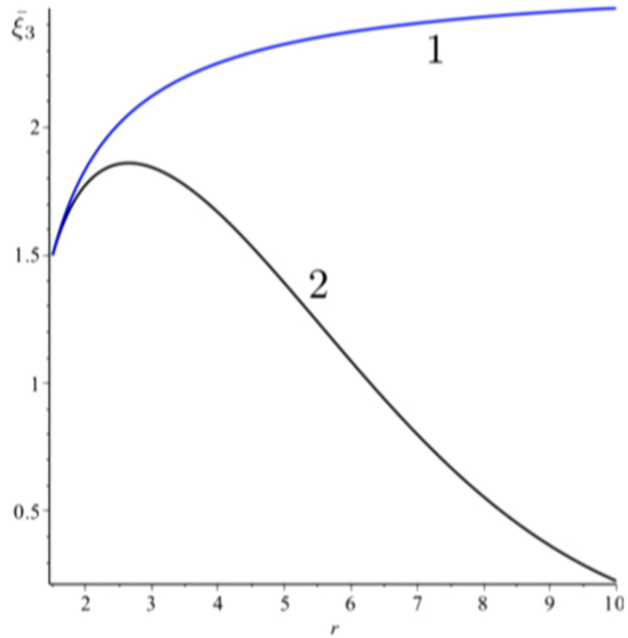

Figure : $\bar{\xi}^3$ as a function of the position of the observer in the equatorial plane.The blue, (1), colour corresponds to the undistorted case whereas the black, (2), colour corresponds to the distorted one. The value of $c_2 = 1/150$.

Results and Discussion: Even multiple moments

In our case metric represents a vacuum space-time, there must be matter sources causing distortion of the black hole outside the region interest. One could extend the solution beyond this (non-vacuum) region to a yet more distant vacuum region. In that case, the expansions of the functions $\mathcal{U}$ and V should be replaced by expansions in terms of exterior multiple moments.

Then, $f\Big|_{r\to\infty} = 1$.

$$+$$

The angular momentum of the photon is conserved as it is traced backward all the way to the black hole.

$$=$$

An observer located at infinity $\bar{\xi}^3$ is larger than that of the undistorted Schwarzschild black hole.

Summary

→In many astrophysical situations, such as a black hole in a binary system, the black hole is distorted.
→Light rays emitted from sources behind the black hole will either be absorbed by it or escape to an observer located at some finite distance (r_o, θ_o) from the black hole. The boundary of the set of rays reaching this observer defines the "local shadow" of the black hole for this observer.
→We computed the local shadow for a distorted Schwarzschild black hole by tracing back the trajectory of photons emitted from a point located on a sphere of radius r_e.
→The parameters $(\bar{\xi}^2, \bar{\xi}^3)$ are related to the initial velocity θ', integral of motion l_z, and the position of the observer.

Summary

→For an octupole distortion $c_1 = -c_3$, we observe an "eyebrow" structure for large values of multiple moments (e.g. $c_1 = 1/800$), reminiscent of those seen for the shadow of two merging black holes [R. Cowen, (2014)].
→For an observer in the equatorial plane the shadow looks like an incomplete ellipse that is flattened on one side.
→Mirror-reflected with respect to the $\bar{\xi}^3$ axis upon changing the sign of the multipole moment from positive to negative.
→The "eyebrow" has the same shape as the "primary shadow ". However, is smaller and a mirror reflection of the "primary image " with respect to $\bar{\xi}^3$.

Summary

→For a quadrupole distortion, c_2 we found that the shadow was deformed from a circle to an ellipse.
→c_2 increases, the shadow gets increasingly deformed.
→ If $c_2 > 0$ the shadow is prolate whereas the horizon is oblate.
→ If $c_2 < 0$ the reverse occurs, with a prolate horizon having an oblate shadow.
→ We have shown analytically why this phenomenon occurs for a local observer.
→ An observer at infinity will see the apparent shape of an oblate black hole (i.e., its shadow) to be either oblate or a circle of greater radius than for the undistorted case.
→ The horizon is very rigid, i.e., it is harder to deform the horizon and easier to have a deformed shadow.

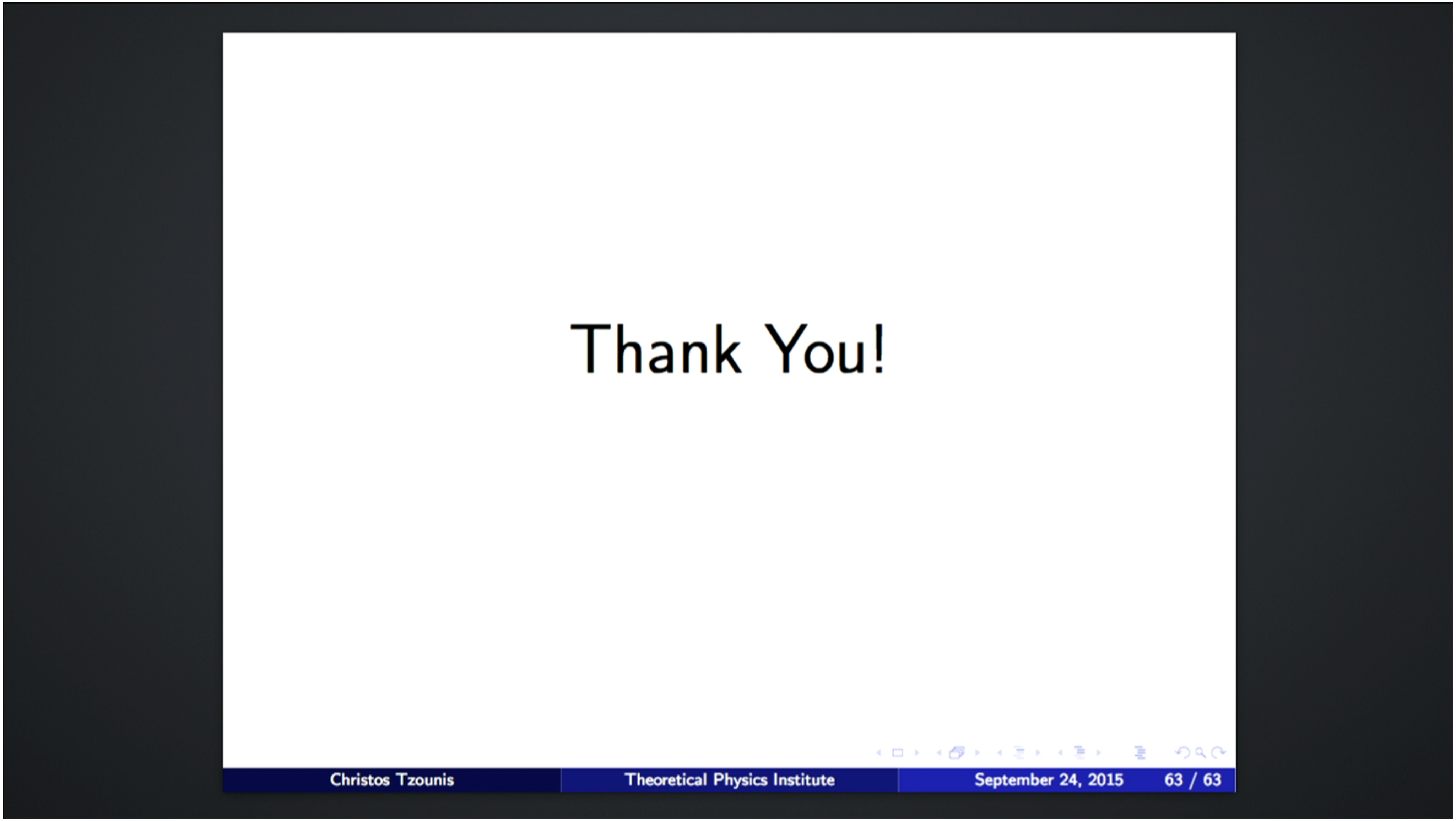
Thank You!
Christos Tzounis
Theoretical Physics Institute
September 24, 2015
63 / 63